Folic Acid-functionalized Graphene Oxide Nanosheets via Plasma Etching as a Platform to Combine NIR Anticancer Phototherapy and Targeted Drug Delivery

Nicolò Mauro[ab]*, Cinzia Scialabba[a], Simonpietro Agnello,[c] Gennara Cavallaro[a], Gaetano Giammona[ad]

[a] Laboratory of Biocompatible Polymers, Department of "Scienze e Tecnologie Biologiche, Chimiche e Farmaceutiche" (STEBICEF), University of Palermo, Via Archirafi 32, 90123 Palermo, Italy.

[b] Fondazione Umberto Veronesi, Piazza Velasca 5, 20122 Milano, Italy

[c] Department of "Fisica e Chimica Emilio Segrè", University of Palermo, Via Archirafi 36, 90123 Palermo, Italy

[d] Institute of Biophysics, Italian National Research Council, Via Ugo La Malfa 153, 90146 Palermo, Italy.

***Corresponding Author:**

E-mail: nicolo.mauro@unipa.it. Fax: +39 09123891928. Tel.: +39 09123891928

Abstract

PEGylated graphene oxide (GO) has shown potential as NIR converting agent to produce local heat useful in breast cancer therapy, since its suitable photothermal conversion, high stability in physiological fluids, biocompatibility and huge specific surface. GO is an appealing nanomaterial for potential clinical applications combining drug delivery and photothermal therapy in a single nano-device capable of specifically targeting breast cancer cells. However, native GO sheets have large dimensions (0.5-5 μm) such that tumor accumulation after a systemic administration is usually precluded. Herein, we report a step-by-step synthesis of folic acid-functionalized PEGylated GO, henceforth named GO-PEG-Fol, with small size and narrow size distribution (~30±5 nm), and the

ability of efficiently converting NIR light into heat. GO-PEG-Fol consists of a nano-GO sheet, obtained by fragmentation of GO by means of non-equilibrium plasma etching, fully functionalized with folic acid-terminated PEG_{2000} chains through amidic coupling and azide-alkyne click cycloaddition, which we showed as active targeting agents to selectively recognize breast cancer cells such as MCF7 and MDA-MB-231. The GO-PEG-Fol incorporated a high amount of doxorubicin hydrochloride (Doxo) (> 33%) and behaves as NIR-light-activated heater capable of triggering sudden Doxo delivery inside cancer cells and localized hyperthermia, thus provoking efficient breast cancer death. The cytotoxic effect was found to be selective for breast cancer cells, being the IC_{50} up to 12 times lower than that observed for healthy fibroblasts. This work established plasma etching as a cost-effective strategy to get functionalized nano-GO with a smart combination of properties such as small size, good photothermal efficiency and targeted cytotoxic effect, which make it a promising candidate as photothermal agent for the treatment of breast cancer.

Keywords: Graphene oxide, breast cancer, doxorubicin, folic acid, phototherapy

1. Introduction

Breast cancer (BC) is the most common disease in women and current drug therapies are far from optimal.[1] Many severe side effects arise from therapeutic strategies to treat BC, sometimes combined with low effectiveness and poor bioavailability once cancer metastasizes.[2,3] This because cancer treatments rely on the use of drugs whose inherent antineoplastic effect is directly related to the way by which it is distributed and delivered into specific body districts.[4,5] Drug delivery systems could affect drug bioavailability, distribution and toxicity, thereby ensuring a key role in developing more selective and efficient cancer treatments.[6] Besides, considerable attention is being focused on smart nanomedicines which combine photothermal therapy and targeted drug delivery, as they are multieffect tools to overcome drug resistance shortcoming.[7–9]They are photosensitizing agents able to enter cancer cells to generate heat from near-infrared (NIR) light absorption, yielding to photothermal

ablation of solid tumors coupled with selective drug release inside cancer cells. Among these, graphene oxide-based nanomedicines are endowed with a combination of biological and optical properties potentially useful to deliver high amounts of anticancer drugs to the site of action and, simultaneously, act as photosensitizer to increase the anticancer efficacy of these compounds.[10–12]

From a chemical standpoint graphene oxide (GO) is a monoatomic layer of sp^2 hybridized carbons statistically sp^3 hybridized and functionalized with oxygen-containing functional groups on its surface (epoxy, hydroxyl and carboxyl groups) which serve as precursors for further derivatization, which enables the use of bioactive molecules (e.g., targeting agents, prodrugs and antibody) leading to enhanced tumor tissue retention without any noticeable toxic effect.[13–15] In fact, to avoid undesired heating of healthy cells, surface functionalization of GO with targeting agents such as biotin or folic acid would lead to selective uptake in breast cancer cells overexpressing specific receptors instead of normal cells in healthy tissues. GO has attracted great attention in the development of cancer nanomedicine because of its ability to not only improve the loading and pharmacokinetic of anticancer drugs, but also to release the drug payload at a controlled rate by light-activated photothermal processes.[16–20] The release of a high localized dose of active compounds inside tumors avoids the aforementioned limitations associated with the poor bioavailability and, as consequence, the multidrug resistance phenomena.[10,21,22]

Among materials currently under investigation with high potential as photothermal agents in the NIR region, including gold nanorods, carbon nanotubes and carbon nanodots, GO has been recently proven able to play itself an essential role in the inhibition of cancer cells propagation *in vitro*.[23–27] It has been showed that GO induces membrane destabilization and oxidative stress in cancer cells leading to apoptosis as well as the potential to act as a chemo-sensitizer for cancer cell treatment, since it provokes autophagy in mouse CT26 cancer cells by activating toll-like receptors.[28–30] Besides, Zhou et al. have found that poly(ethylene oxide)-functionalized GO (PEG-GO) can trigger the downregulation of many mitochondrial proteins which inhibits breast cancer metastasis *in vivo*.[31]

The awareness of these literature data led us to suppose that GO nanosheets bearing PEG_{2000} chains and folic acid pendants, used as active targeting agent, might selectively enter breast cancer cells overexpressing folic acid receptors (FRs) to release the drug payload in a NIR-sensitive fashion, and synergistically perform its inherent anticancer effect to provoke tumor death. Herein, we developed nano-sized GO with narrow size distribution, and highly functionalized with PEG chains bearing folic acid as end-chain. The GO nano-flakes were obtained by the fragmentation of common GO flakes (~0.5-5 μm length) via low vacuum plasma etching, affording dimension of about 30 nm. The potential as anticancer agent in targeted photothermal therapy was established on MCF7, MDA-MB-231 and HDFa cell lines, used as breast cancer and healthy cells, respectively.

2. Materials and methods

2.1 Materials

Doxorubicin hydrochloride (Doxo), N-hydroxysuccinimide (NHS), 1-ethyl-3-(3-dimethylaminopropyl)-carbodiimide hydrochloride (EDC-HCl), 4-pentynoic acid (CC), copper (II) sulfate pentahydrate, ascorbic acid (99%), folic acid (99%) and poly(ethylene glycol) bis(amine) Mw 2,000 were purchased from Sigma Aldrich. The reagents were of analytic grade and used as received. Graphene oxide (GO) was purchased from ACS Material (USA) and used after purification by dialysis tube with nominal molecular weight cut off 10^6 Da. SpectraPor dialysis tubing was purchased from Spectrum Laboratories, Inc. (Italy).

^{1}H NMR spectra were recorded using a Bruker Avance II 300 spectrometer operating at 300.12 MHz.

Size exclusion chromatography (SEC) was carried out using Tosho Bioscience TSK-Gel G4000 PWXL and G3000 PWXL columns connected to a Water 2410 refractive index detector. The mobile phase was a 0.1 M Tris buffer pH 8.10± 0.05 with 0.2 M sodium chloride. The flow rate was 0.8 mL min^{-1} and sample concentration 3 mg mL^{-1} and PEG standards (100-0.400 kDa, Polymer Laboratories Inc., USA) were used to set up calibration curve (R^2 = 0.996).

Human fibroblasts (HDFa), breast cancer MCF-7 and MDA-MB-231 cells (purchased from Istituto Zooprofilattico Sperimentale della Lombardia e dell' Emilia Romagna, Italy) were grown in Dulbecco's modified Eagle's medium (DMEM) supplemented with 10% v/v Fetal Bovine Serum (FBS), 2 mM L-glutamine, 100 units/mL penicillin G, 100 µg/mL streptomycin at 37°C and 5% CO2.

2.2 Synthesis of folate-PEG-4-pentynoic acid derivative (Fol-PEG-CC)

Amino-PEG-Folate (NH_2-PEG-Fol) (200 mg) was obtained as reported elsewhere and solubilized in ultrapure water (10 mL).[16] To this solution in turn 4-pentynoic acid (13.6 mg, 0.139 mmol) and, subsequently, EDC-HCl (26 mg, 0.139 mmol) and NHS (16.0 mg, 0.139 mmol) were added with vigorous stirring. The pH of the reaction was adjusted to 6.4 and maintained for 45 minutes. After this time, the reaction was kept at room temperature for 18h. Then the heterobifunctional Fol-PEG-CC was separated from by-products through gel filtration chromatography (Sephadex ® G15, ultrapure water as eluent, flow 1.2 mL min^{-1}). Yield 89%.

^{1}H NMR (300.15 MHz, MeOD-d_4): δ_H 2.09 (1H, s, -CC**H**$_{alkyne}$), 2.51 (4H, br., -COC**H$_2$**C**H$_2$**CH-), 2.19 – 2.60 (6H, m, -CONHC**H$_2$**C**H$_2$**NH- and -OCOC**H$_2$**CH_2NH-), 2.84 (4H, br., -C**H$_2$**C**H$_2$**CCH), 3.74 (183H, s, OC**H$_2$**$_{PEG2000}$ and -OC**H$_2$**CH_2OCO-), 6.68 (2H, m, m-C**H**$_{folic\ acid}$ aromatic ring), 7.63 (2H, m, o-C**H**$_{folic\ acid}$ aromatic ring), 8.76 (1H, s, C**H**$_{folic\ acid}$ heteroaromatic ring)

Size exclusion chromatography (SEC): M_W = 2560, Mn = 2150, PD = 1.19

2.3 Synthesis of GO-N_3 nanoflakes

Graphene oxide (20 mL, 7.5 mg mL^{-1}) was added to a solution of sodium azide (135 mg, 2.08 mmol) in water (13 mL) and the pH was adjusted to 8.5±0.1 using 1 N sodium hydroxide. The dispersion was kept at room temperature for 1h and then freeze-dried.[32] The crude powder was treated with nitrogen plasma (1W, 15 cps, 10 rpm, 10^{-2} mbar) for 40 min. After that, the powder was immediately dispersed in ethanol/water 75:25 by sonicating for 5 minutes (3 times) and maintained at room temperature for

18h. Then the dispersion was sonicated for 3h in an ice bath, diluted to 150 mL with water and filtered through a syringe filter with cut off 5 μm. Yield: 89%.

2.4 Synthesis of PEG-Folate functionalized GO nanoflakes (GO-PEG-Fol)

The dispersion of GO-N_3 nanoflakes previously obtained (10 mL, 10 mg mL^{-1}) was added dropwise with stirring to an aqueous solution of NH_2-PEG-Fol (200 mg; 0.098 mmol) at pH 6.4. EDC (25 mg, 0.130 mmol) and NHS (14.96, 0.130 mmol) were then added at once and the pH kept within 6.2-6.5 for 4 h under sonication in an ice bath (17-22 °C). Then the reaction proceeded for 18 h at room temperature with stirring. After that it was sonicated for 2 h in an ice bath. Finally, in turn Fol-PEG-CC (Mw = 2391; Mn = 2152; 200 mg; 0.087 mmol), ascorbic acid (10 % w/w) and copper (II) sulfate (5% w/w) were added. After 6 h the reaction was dialyzed through a membrane with cut off 25 k and the product retrieved as brown slurry. Yield 81%

2.5 Atomic force microscopy (AFM) of GO-PEG-Fol

AFM imaging was carried out as previously reported.[17] A drop of a suspension of GO-PEG-Fol in ultrapure water (10^{-4} mg mL^{-1}) was deposited onto a mica disk and then dried under vacuum (20 mbar) overnight. AFM measurements were performed in Tapping mode by a Bruker Dimension FastScan microscope equipped with closed-loop scanners and using a FastScan A probes (resonance frequency = 1400 kHz, tip radius = 5 nm).

Furthermore, in order to study the etching kinetics, for the GO-N_3 samples AFM measurements were recorded before and after 120 and 240 minutes from the treatment with nitrogen plasma.

2.6 Scanning Electron Microscopy (SEM) Analysis

To study the morphology of the GO-PEG-Fol nanoflakes the freeze-dried sample was observed using a FEI Quanta 450 Scanning Electron Microscope. Samples were deposited on a double sided adhesive tape previously applied on a stainless steel stub. GO-PEG-Fol nanoflakes were then sputtered with gold prior to microscopy examination.

2.7. Raman spectroscopy

MicroRaman measurements have been carried out by a Horiba LabRam HR-Evolution multiline spectrometer employing the 532 nm laser excitation. A drop of the given GO solution was deposited on an Al plate and after solvent evaporation at room temperature measurements have been carried out. The laser power was fixed at 0.1 mW, to avoid sample modification, and the spectral resolution was 7 cm^{-1}. The area investigated by the single measurement using a 100x magnification objective was 1 μm^2.

2.8 Dynamic light scattering (DLS) measurements and ζ-potential analysis

DLS analyses and ζ-potential measurements (mV) were performed at 25° C using a Malvern Zetasizer NanoZS instrument, fitted with a 532 nm laser at a fixed scattering angle of 173°. Either GO-PEG-Fol or Doxo-loaded GO-PEG-Fol nanoflakes (0.2 mg mL^{-1}) was dispersed in ultrapure water by sonicating and filtered through a 5 μm cellulose membrane syringe filter before performing the analysis. The Z-average and polydispersity index (PDI) were obtained by cumulates analysis of the correlation function. The ζ-potential (mV) was calculated from the electrophoretic mobility using the Smoluchowski equation and assuming that Ka >> 1 (where K and a are the Debye–Hückel parameter and particle radius, respectively).[33]

2.9 Evaluation of the hyperthermic effect of GO-PEG-Fol nanoflakes

A dispersion of GO-PEG-Fol nanoflakes in water (20 mL, 0.5mg mL^{-1}) was prepared and treated with a 810 nm diode laser (GBox 15A/B by GIGA Laser) with the power fitted at either 0.5 or 1.4 W cm^{-3}. At fixed intervals the temperature of the dispersion was recorded and reported as a function of the exposure time. The same experiment was carried out on Milli-Q water as blank.

2.10 Drug loading and drug release kinetics

The amount of doxorubicin loaded in GO-PEG-Fol/Doxo was determined spectrophotometrically, extracting Doxo from the GO-PEG-Fol/Doxo (4 mg) with 0.1 M phosphate buffer at pH 7.4 (20 ml) by sonicating and measuring the absorbance of the extract at 480 nm. The amount of Doxo was calculated

using a calibration curve obtained from standard solutions of Doxo in 0.1 M phosphate buffer at pH 7.4 (concentration range from 10^{-4} to 0.5 mg mL^{-1}; R^2 = 0.999). The content of doxorubicin was expressed as the amount of loaded doxorubicin hydrochloride per unit mass of nanosystem, and resulted to be 33.3 ±0.3%.

For the drug release studies in artificial medium, GO-PEG-Fol/Doxo (3.0 mg) was dissolved in PBS at pH 7.4 (5 mL) and placed into a dialysis tubing with a MWCO 2 kDa. It was then immersed into PBS at pH 7.4 (40 mL) and incubated at 37 °C under continuous stirring (100 rpm) in a Benchtop 808C Incubator Orbital Shaker model 420, for 48 h. Aliquots of the external medium (1 mL) were withdrawn from the outside of the dialysis tubing at scheduled time intervals and replaced with equal amount of fresh medium. The amount of Doxo released was evaluated measuring the absorbance of each sample as above described. The cumulative release was determined as a function of incubation time. Drug release experiments were also carried out using PBS pH 5.5. All release data were compared with the diffusion profile of doxorubicin hydrochloride alone (0.5 mg) obtained by using the same procedure. Data were corrected taking in account the dilution procedure. Results were reported as average values of three different experiments and in agreement within ±5% standard error. The hyperthermia-triggered drug release was evaluated treating a suspension of GO-PEG-Fol/Doxo previously incubated for 4 h in PBS pH 7.4 with a 810 nm laser (power fitted at 7×10^{-2} W mm^{-3}) for 200 s and comparing the release values with that observed for the untreated control after an incubation time of 4 h in PBS pH 7.4.

2.11 In vitro cytotoxicity study of GO-PEG-Fol/Doxo

The cytotoxicity of GO-PEG-Fol/Doxo was assessed by the MTS assay on human breast cancer cell lines (MCF-7 and MDA-MB-231) and healthy human fibroblast (HDFa) using a commercially available kit (Cell Titer 96 Aqueous One Solution Cell Proliferation assay, Promega). Cells were seeded in a 96-multiwell plate at a density of 1×10^4 cells/well and grown in DMEM. After 24h, the medium was replaced with 200 μL of fresh culture medium containing GO-PEG-Fol/Doxo at different

concentrations, corresponding to equivalent concentrations of Doxo of 0.1, 0.5, 1, 2.5, 5 and 10 μM. After 24 and 48 h, samples were withdrawn from the wells and replaced with fresh medium (100 μL) and 20 μL of a MTS solution. Cells were incubated for additional 2 h at 37 °C, and then the absorbance at 490 nm was measured using a microplate reader (Multiskan, Thermo, U.K.). Free Doxo solutions at the same concentrations were used as a positive control, as pure cell medium was used as a negative control. Additional experiments were accomplished to evaluate the hyperthermic effects of GO nanoflakes. In particular, HDFa, MCF7 and MDA-MB-231 cell lines were incubated with either GO-PEG-Fol/Doxo or free Doxo for 24 h and then were irradiated with a 810 nm laser beam for 200 sec. After the laser treatment, DMEM was removed, cells washed up twice with DPBS and cells viability evaluated by MTS assay as above-described. Laser treated cells were used as a negative control. Moreover, LIVE/DEAD Cell Viability Assays (Thermo Fischer) was carried out on cells lines treated with 5 μM of DOXO or equivalent amount of GO-PEG-Fol, and images were recorded by a fluorescence microscope using an Axio Cam MRm (Zeiss).

Results were expressed as percentage reduction of the control cells. All culture experiments were performed in triplicates.

2.12 Cell uptake study of GO-PEG-Fol on healthy and breast cancer cell lines

The cellular uptake of GO-PEG-Fol nanoflakes was assessed by fluorescent microscopy (Zeiss "AXIO Vert. A1" Microscope Inverted) on HDFa, MCF-7 and MDA-MB-231 cells (2.5×10^4 cells/well) cultured for 24 h. [34] Briefly, each well was treated with 500 μL of fresh DMEM containing 5 μM Doxo or equivalent amount of GO-PEG-Fol/Doxo and cells were incubated for 2-4-6-24 h. Thus, the medium was removed, the cell monolayer was washed twice with PBS pH 7.4, and the nuclei were stained with 4′,6-diamidino-2-phenylindole (DAPI). Images were recorded by a fluorescence microscope using an Axio Cam MRm (Zeiss). Untreated cells were used as negative control to set the auto fluorescence.

2.13 In vitro wound healing assay (cell migration test)

The ability of GO-PEG-Fol/Doxo to reduce cell migration was evaluated by the scratch assay. A monolayer of either HDFa, MCF-7 and MDA-MB-231 was cultured in 48-well plates at a density of 5 × 10^4 cells/well for 48h, and then a wound space was created with a p200 pipet tip. Cells were washed up with DMEM to remove the debris and smooth the edge and then incubated with 5 μM Doxo or equivalent amount of GO-PEG-Fol/Doxo. Untreated cells were used as positive control. After 24 and 48 h of incubation cells were washed with PBS pH 7.4 and micrographs were taken with an optical microscope equipped with a digital camera (Axio Cam MRm, Zeiss). The cell-to-cell gap was measured using Zeiss acquisition software.

3. Results and discussion

3.1 Synthesis of folate-PEG-4-pentynoic acid derivative (Fol-PEG-CC)

In recent past, PEGylation strategy has attracted much attention in the field of surface chemistry applied to nanomedicine, due to its biocompatibility, solubility and flexibility that induce stability and stealth properties to drug delivery systems in the blood compartment. In fact, PEGylation allows avoiding the interaction between blood elements and the surface of the coated systems, thus promoting higher biocompatibility and long bloodstream circulation owing to the limited capture by the mononuclear phagocyte system (RES) [35]. Here, in order to prepare nano-sized GO flakes with PEGylated surface, heterobifunctional polyethylene oxides (PEGs) (Mw = 2100, PD = 1.34) bearing folic acid at one end and propargylacetic (Fol-PEG-CC) or amine (Fol-PEG-NH_2) group at the other end-chain were employed. Folic acid was chosen as active targeting agent, since it has been widely demonstrated his capability to bind, with high affinity, FA receptors overexpressed in several human carcinomas such as ovary, breast, colon, lung, brain, and endometrium cancers.[36] [37] Whereas PEG_{2000} was selected because it is a discrete high mobile macromolecule that generates large volume exclusion that limits unspecific protein adsorption *in vivo* and proven able to allow specific recognition

of targeting agents introduced as end-chain.[38] The alkyne-terminated PEG-Fol was exploited to functionalize both faces of GO-N_3 by the click reaction between azides of GO-N_3 and alkyne end chain of Fol-PEG-CC, while the amine-teminated PEG was introduced at the GO perimeter by the coupling reaction between carboxyl groups of GO-N_3 and the amine function of the PEG chains.

The synthesis of the Fol-PEG-CC was carried out by two synthetic steps with isolation and purification of the NH_2-PEG-Folate intermediate (Scheme 1). In the first step the bis-amino-PEG, with a molecular weight of 2 kDa (PD = 1.28), was functionalized at one end-chain with folic acid by amidic bond using EDC and NHS as activating agents. An excess of folic acid (1.2 eq.) was used to avoid the presence of the unreacted telechelic product so as to facilitate the work up. Under these reaction conditions both the

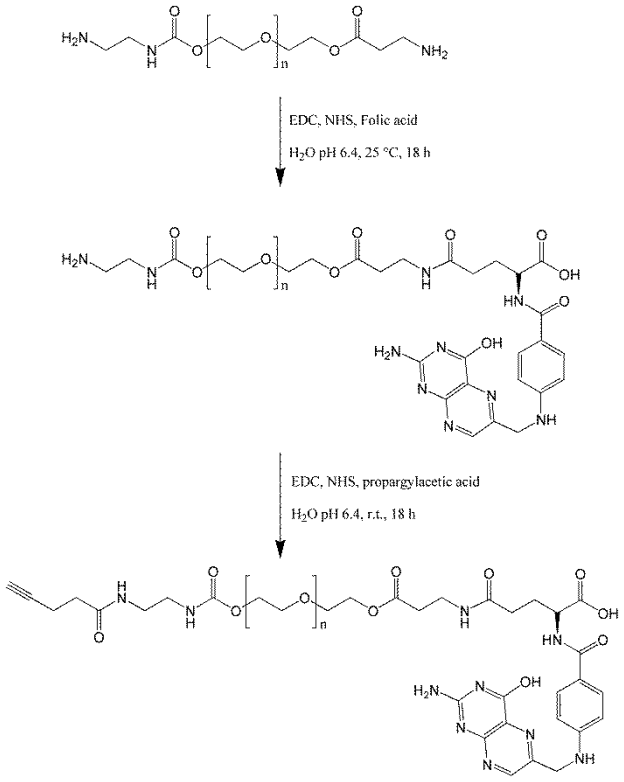

Scheme 1. Schematic representation of the synthetic pathway employed for the synthesis of Fol-PEG-CC.

telechelic product of bis-addition and the semitelechelic product of interest (NH_2-PEG-Fol) are formed proportionally to the amine/carboxyl acid ratio used.[39] The molar ratios used allowed obtaining 90 % of the mono-functionalized derivative on a molar basis. NH_2-PEG-Fol was isolated after purification

by SEC using a G15 resin able to efficiently separate semitelechelic PEG chains from other by-producs. The hypothesized structure of NH_2-PEG-Fol was confirmed by ^1H NMR spectroscopy (Figure 1). In particular, the characteristic resonances at 6.68-8.76 ppm of the proton of the folic acid aromatic and heteroaromatic rings, together with the shift of the proton resonances at 2.19-2.60 ppm ascribable to the terminals, suggest a successful derivatization of PEG chains at the end-chain. Moreover, the derivatization degree of folic acid, calculated by comparing the normalized integrals of the peaks at 6.68 ppm with that at 3.74 ppm, was found to be 2.26% on a molar basis (1:45 repeating units), consistent with a PEG molecule functionalized only at one end-chain.

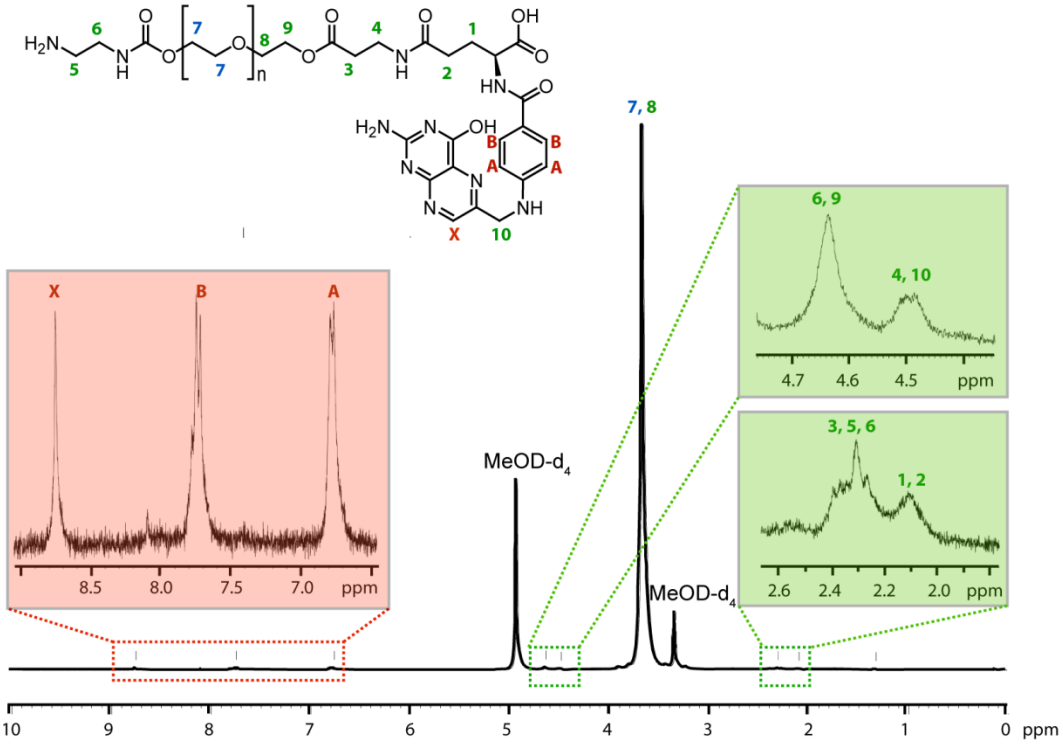

Figure 1. ^1H NMR (300.15 MHz) spectrum of the NH_2-PEG-Fol in MeOD-d_4

In the second step the NH_2-PEG-Fol intermediate was derivatized with an alkyne group, and in particular with propargylacetic acid, with the aim of obtaining a heterobifunctional PEG able to react orthogonally with the azide groups present on the surface of the graphene oxide synthesized, instead of with the carboxylic functions at the GO perimeter. With this in mind, the amine group of NH_2-PEG-Fol was conjugated with the carboxylic group of propargylacetic acid using EDC and NHS as coupling

agents. In this reaction the likelihood that PEG-PEG cross-coupling occurred, due to the presence of the folate free carboxylic group, was negligible. In fact, the extremely high steric hindrance of the alpha carboxylic acid in the folate residue provides poor reactivity and, coupled with the high competition caused by the use of excess of propargylacetic acid (2 eq.), allowed yielding to exclusive formation of the heterobifunctional PEG of interest (Fol-PEG-CC). The structural identification of Fol-PEG-CC was attained by ^{1}H NMR. Apart from the typical groups of resonances observed for the parent compound, the alkyne hydrogen resonance at 2.09 ppm confirmed the functionalization of the amine end-chain with the alkyne moiety. The derivatization degree in propargylacetic acid was calculated comparing the integral of the methine proton (1H) observed at 2.09 ppm with that of the protons noticed at 3.74 ppm, attributable to the methylene of the PEG repeating units (176H). This was 2.21% on a molar basis (1:45 repeating units), the same observed for the other end-chain (folic acid), in agreement with the structure expected for the heterobifunctional Fol-PEG-CC macromolecule.

3.2 Synthesis and characterization of GO-PEG-Fol nanoflakes

PEGylation of GO usually involves the coupling reaction between their outside carboxylic functions with compounds containing amines such as polyamines, polyampholytes or proteins. However, in such nanosystems both faces remain largely free to adsorb proteins in vivo, which is reflected in a low biocompatibility. In addition, the low derivatization degree in targeting agents arisen from these high localized reactions usually limits water stability in physiological fluids and impede an efficient receptor-mediated cell uptake, thus a successful targeted cancer therapy can be jeopardized. In principle, the epoxy groups of the GO surface can be used for covalent bonding and hence to obtain highly PEGylated GO nanoflakes. Here, GO (monolayer of 500 nm length) was treated with sodium azide to open the epoxide function obtaining the GO-N_3. Hence, the azide groups introduced on GO surface can selectively react with alkyne-functionalized polymers by means of 1-3 dipolar cycloaddition (Scheme 2).

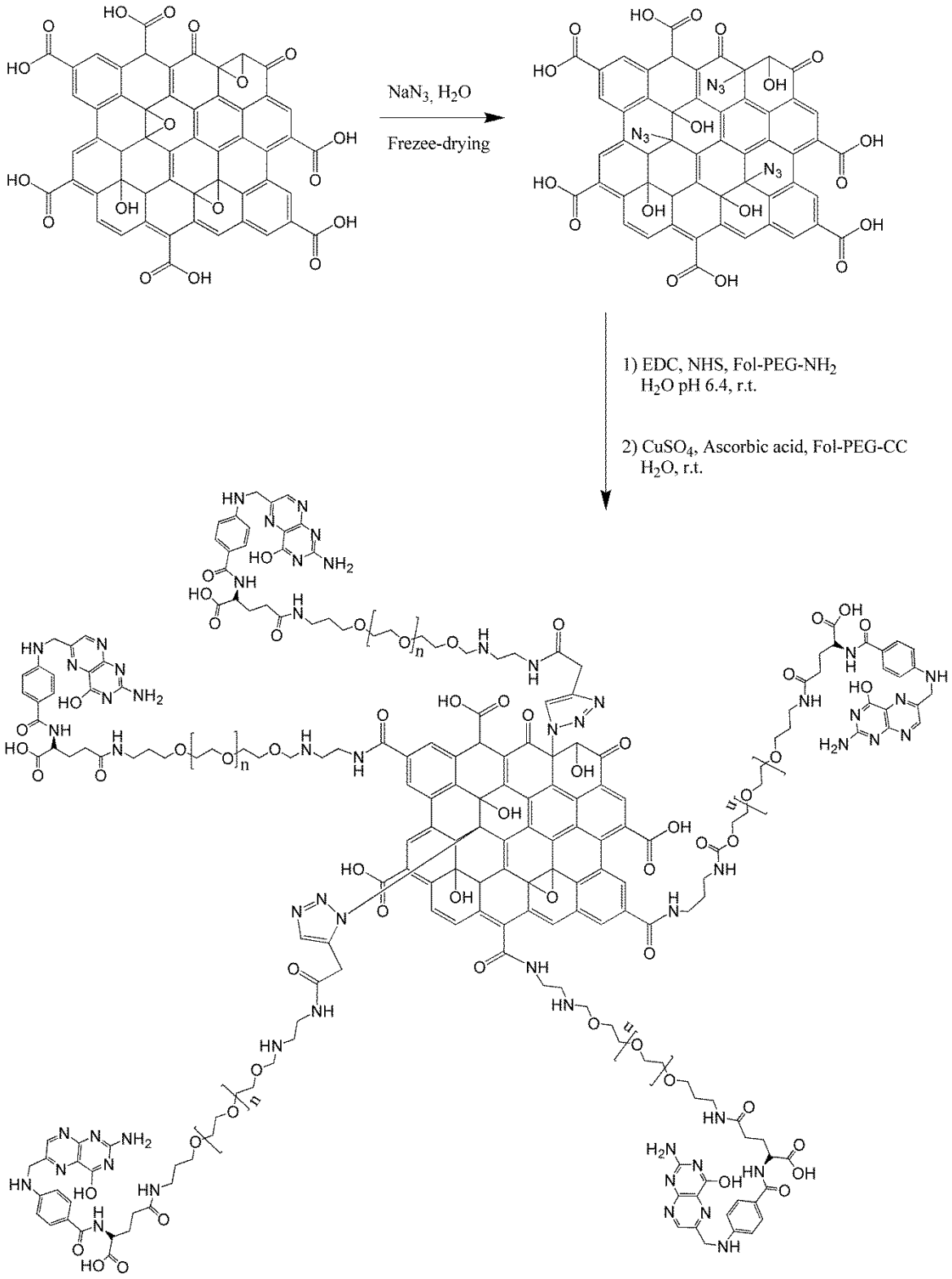

Scheme 2. Synthesis of the graphene oxide-Polyethylene glycol-Folate (GO-PEG-Fol).

The reaction was carried out both by thermal processes, with a reflux, and by a solvent free reaction. The highest degree of conversion was achieved using the solvent free reaction conditions.[40] In particular, the graphene oxide was mixed with sodium azide, and then water was removed by freeze-drying. Under these conditions, sodium azide is able to react with the epoxides exposed on the surface of the GO allowing a good functionalization, as confirmed by the presence of the typical band at 2168 cm^{-1} in the infrared spectrum (S1).

Nano-sized GO-N_3 flakes were obtained via plasma etching, using nitrogen plasma in a capacitive reactor operating at low vacuum. Being slightly corrosive, nitrogen plasma is able to etch GO sheets thus reducing original dimensions. Figure 1 shows AFM micrographs of the GO-N_3 derivative before (Fig. 2a) and after the plasma treatment (Fig. 2b-c). AFM micrographs displayed that the plasma treatment induces the formation of grooves in the center of GO-N_3 flakes and the formation of small fragments of GO-N_3 of about 30 nm (Fig. 2b). The reaction evolves over 240 minutes after the plasma treatment to lead to nano-flakes of about 30-40 nm width and 1 nm thickness (Fig. 2c), attributable to GO-N_3 monolayers with narrow size distribution.

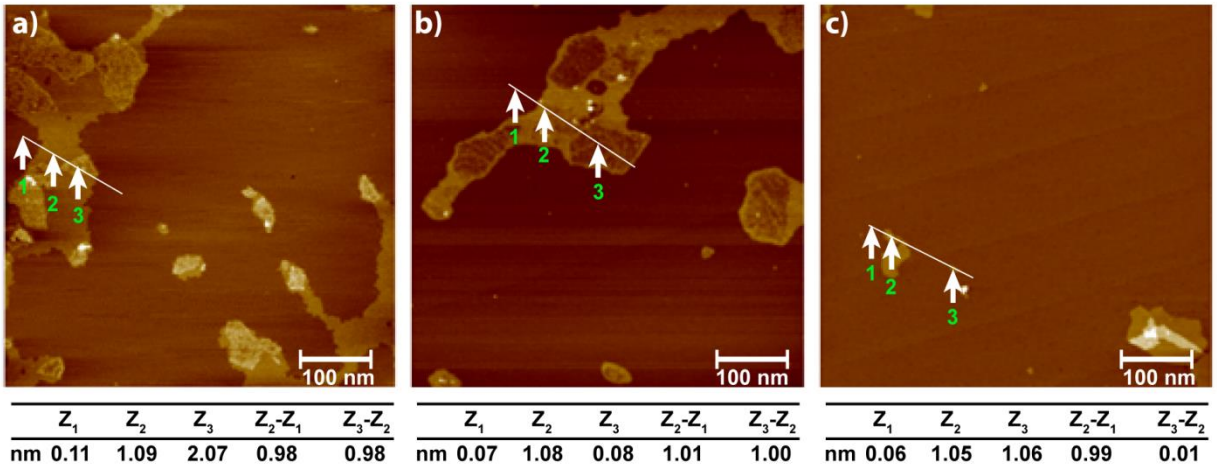

Figure 2. AFM micrographs of the pristine GO-N_3 (a) and the nitrogen plasma-treated GO-N_3 after 120 min (b) and 240 min (c) from the treatment.

The Raman measurements reported in Figure 3 evidences that no relevant changes in the GO structure are induced by the plasma treatments up to 120 minute. In details, both the D,G spectral region around 1500 cm^{-1} and the 2D region at about 2900 cm^{-1} feature the typical bands of GO with negligible amplitude and position modifications.[41]

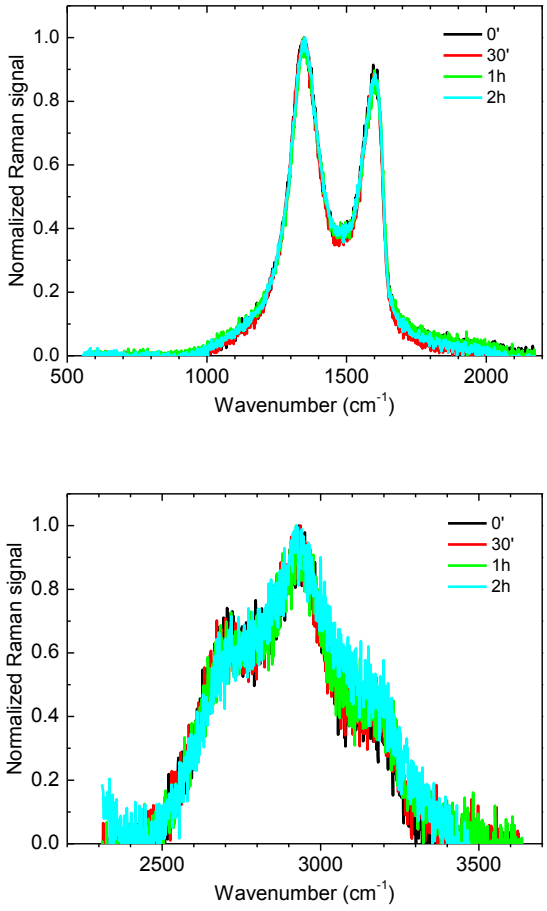

Figure 3. Raman measurements of the GO-N_3 before and after nitrogen plasma treatment up to 120 min.

The GO-N_3 nanoflakes were further derivatized with Fol-PEG-CC and NH_2-PEG-Fol to obtain a nanosystem endowed with high stability in physiological fluids and capability of actively recognizing tumor cells. The greater stability of the nanosystem was achieved by means of a full PEGylation of both the perimeter and the two mirror faces of the GO-N_3 nanoflakes (Scheme 2). While the perimeter

of the GO-N_3 nanoflakes bears carboxylic acid functions capable of reacting with the amine groups of NH_2-PEG-Fol upon activation with EDC and NHS, both planar faces contain azide groups able to chemo-selectively react with the alkyne group of Fol-PEG-CC. It was not necessary to purify the product before carrying out the latter reaction step, since the 1,3-dipolar cycloaddition reaction and the amide coupling reaction were completely orthogonal, obtaining a pure product with high yields (Yield = 98%).

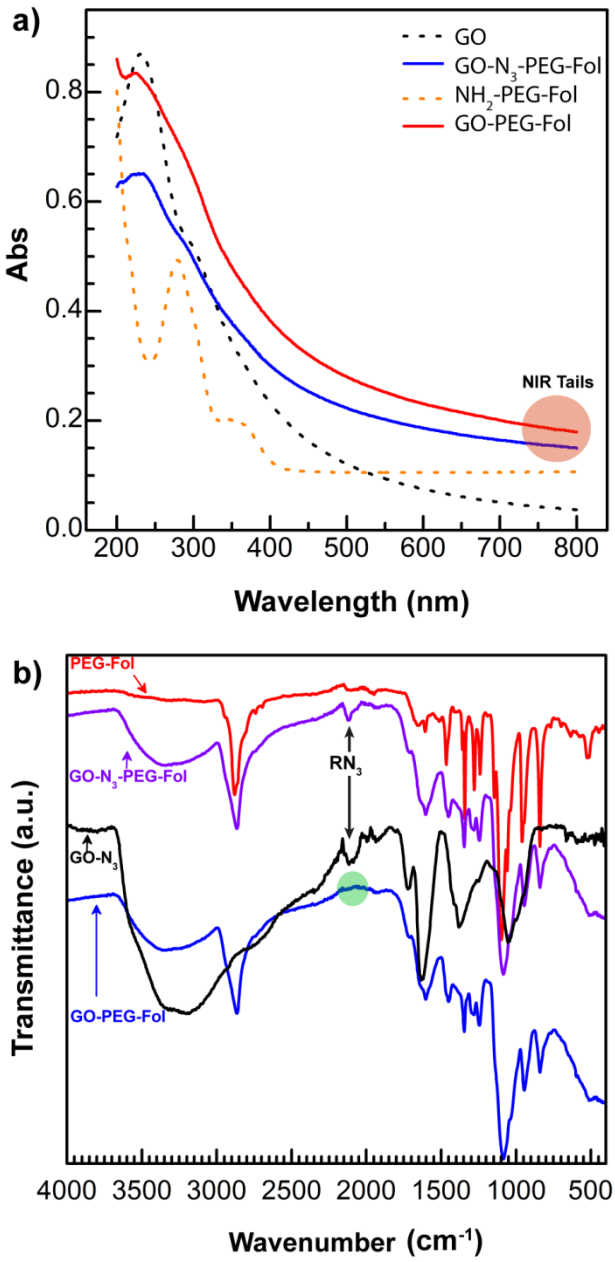

Figure 4. Absorption spectra (a) and FT-IR spectra (b) of GO-PEG-Fol and the parent compounds

A reliable investigation of GO-PEG-Fol structure is by no means trivial, and therefore we used many spectroscopic and microscopic methods to assess the feasibility of the reactions. Figure 4 a depicts the UV spectra obtained for GO-PEG-Fol compared to those of the intermediates. Both GO-N_3-PEG-Fol and GO-PEG-Fol sample displayed the typical absorption bands of NH_2-PEG-Fol at 200, 275 and 355 nm. Furthermore, the contribution of the folic acid bands was much more for the GO-PEG-Fol sample, which confirms the higher derivatization degree of this nanostructure owing to the complete

functionalization of both GO faces. It is noteworthy that the NIR absorption tails for the GO samples increased over the degree of functionalization in folic acid, implying higher photothermal conversion for the GO-PEG-Fol sample. The covalent functionalization of GO-PEG-Fol was also studied by FTIR (Figure 4b). The GO-N_3-PEG-Fol spectrum was characterized by some diagnostic vibrations ascribable to GO sheets, such as those at 3300 cm^{-1} (OH and H_2O stretching), 1750 cm^{-1} (C=O stretching), 1668 cm^{-1} (C=C stretching) and 1611 cm^{-1} (asymmetric COO^- stretching), together with typical bands of CONH-PEG-Fol moiety located at 2880 cm^{-1} (O-CH_2- stretching) and 1615 cm^{-1} (CONH stretching), implying that PEG-Fol moieties are covalently linked to the GO sheets. Besides, not significant changes in the mode of vibrations were observed at 2168 cm^{-1} (azide group), suggesting that the derivatization with PEG-Fol occurred along the flake's perimeter between carboxilyc groups of GO and amine functions of NH_2-PEG-Fol. The disappearance of the latter vibration in the GO-PEG-Fol spectrum, combined with more marked PEG-Fol bands, clearly showed that a further covalent functionalization of GO-N_3-PEG-Fol involved the reaction of alkyne groups of Fol-PEG-CC and azide functions of GO-N_3-PEG-Fol. This is also a good evidence that PEGylation occurred regioselectively at both GO surfaces.

The functionalization of GO sheets with PEG-Fol chains was also established by means of AFM and SEM microscopies (Figure 5). Figure 5a shows a typical dimensional distribution analysis of GO-PEG-Fol, where the presence of GO islands with a thickness of about 3.5 nm and a diameter of about 40 ± 4 nm can be observed. The increase of the nano-flakes thickness of about 2.5 nm can be explained with a homogeneous functionalization of the GO surface with Fol-PEG-CC chains of 2.5 kDa, corroborating UV and FTIR data.[5,42] It might be noticed that the small size and the narrow size distribution observed are suitable for biomedical applications, especially as carrier for anticancer drugs, since nano-carriers with dimensions between 20-50 nm allow enhanced *in vivo* bioavailability and tumor accumulation, thereby improving the effectiveness of anticancer treatments.

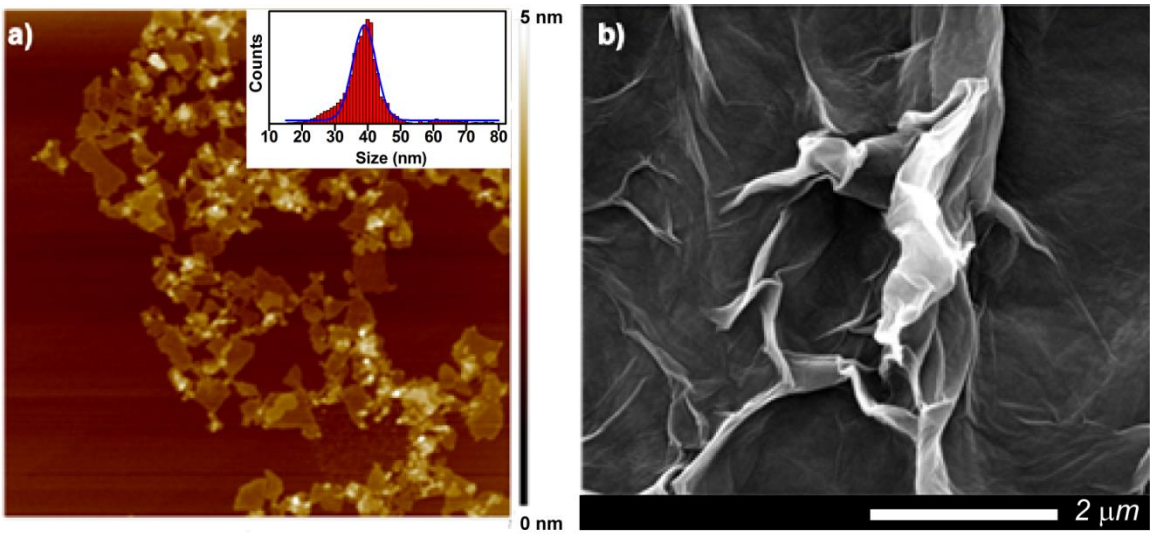

Figure 5. AFM measurement and size distribution (a) and SEM micrograph (b) of GO-PEG-Fol.

SEM analysis of GO-PEG-Fol reported in Figure 5b displayed unilamellar GO sheets with the characteristic structure observed in the native GO flakes, nevertheless exhibiting a roughness attributable to the PEG chains deposited onto the GO surface. On the whole, AFM and SEM data corroborated the hypothesis that GO-PEG-Fol is a fully PEGylated GO carrying covalently linked PEG chains both on the edge and on the surface.

3.3 Physicochemical Properties.

3.3.1. Photothermal conversion of the GO-PEG-Fol.

One interesting property of GO is the capability of giving rise to local heating after near infrared (NIR) laser stimulation. This behavior has been recently exploited for the physical eradication of solid tumors through photothermal therapy and for the photo-triggered local release of high amount of anticancer agents [10,17,18,43,44]. This is a minimally invasive technique, which uses hyperthermia, intended as a local rise in temperature into the tumor mass (usually to 40−45 °C), generated by energy transfer produced during the irradiation of GO with a light of wavelength in the NIR region, to kill selectively

cancer cells. Therefore, the ability of GO-PEG-Fol to convert a NIR energy source into heat was evaluated by applying an 810 nm laser beam with variable power density (0.5 and 1.4 W cm^{-2}) for 300 sec and by measuring the temperature of the dispersions (Figure 6). As a rule, the temperature linearly increased over the laser exposure time both at 0.5 and 1.4 W cm^{-2}, reaching a maximum of 44.5 °C after 300 sec at the higher power density employed. A remarkable power-dependent trend was observed. In fact, the temperature increased about two times faster for the sample irradiated with the higher power density. However, the photothermal conversion of GO-PEG-Fol, reported as normalized differential temperature increase (°C cm^3 W^{-1}), followed a non-obvious direction (Figure 6). In particular, the photothermal conversion was about twice bigger at low power density. This can be explained considering that, at the same concentration, the amount of independent harmonic oscillators which determine modes of vibrations in GO-PEG-Fol are stochastically saturated at lower power density, thereby limiting further thermal dissipation of excess energy. Overall, obtained data show that the functionalization of GO with PEG-Fol did not affect the photothermal properties of the virgin GO, since GO-PEG-Fol is still able to cause sudden and efficient heating when stimulated by a laser source at 810 nm. Accordingly, these data seem to suggest that the nanosystems have photothermal characteristics suitable for *in vivo* phototherapy of solid tumors.

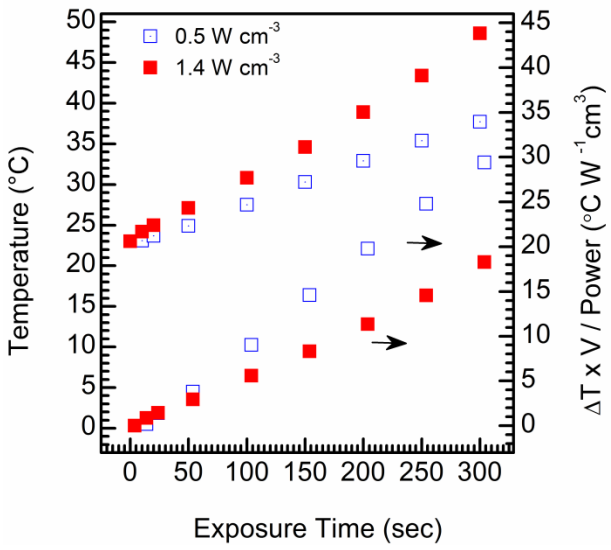

Figure 6. Photothermic behavior of GO-PEG-Fol nanoflakes in water at concentration of 0.5 mg mL^{-1}: temperature (left ordinate) and photothermal efficiency (right ordinate) as function of the exposure time at increasing power density (0.5 and 1.4 W cm^{-2})

3.3.2. Drug loading and drug release studies.

GO nanoflakes are interesting drug carriers because both sides of a single nano-sheet could be accessible for drug binding, offering interesting properties from a technological and pharmaceutical point of view. The high specific surface area and the highly sp2 hybridized structure of GO lead to strong π-π, hydrogen and hydrophobic interactions with aromatic drugs affording to simple adsorption. Many anticancer drugs such as doxorubicin possess aromatic portions useful for their reversible adsorption on GO surfaces, thereby ensuring a gradual and stimuli-sensitive release in the site of action to gain a local therapeutic effect with negligible toxic off-target effects.[45] Therefore, here, the GO-PEG-Fol nano-flakes were loaded reversibly with doxorubicin, used as a model anticancer drug, by simply mixing the drug with the nanosystem under sonication. The Doxo loading was evaluated spectrophotometrically by extracting the drug and measuring the absorbance at λ 480 nm. Results are reported in Table 1.

Table 1. Physiochemical characterization of the GO-PEG-Fol and GO-PEG-Fol/Doxo

Sample	[a]Size (nm)	[a]Thickness (nm)	[a]ζ-Potential (mV)	[c]Drug loading (w/w %)	Loading efficiency (w/w %)
GO-PEG-Fol	35	1.25	-28	n.d.	n.d.
GO-PEG-Fol/Doxo	40	1.3	-5	33.3	98.6

[a] Obtained by AFM analysis

[b] Obtained by DLS analysis

[c] Obtained by spectrophotometric analysis

It is interesting to notice that almost all Doxo incubated whit GO nanoflakes was absorbed, obtaining a drug loading of 33.3 % (w/w) with a loading efficacy of 98.65 %, one of the highest observed in the literature.[46] The ability of GO-PEG-Fol nano-flakes to adsorb Doxo was also confirmed by ζ-

potential measurements. The reduction of the ζ-potential value (from -28 to -5 mV) observed for the GO-PEG-Fol/Doxo sample indicated that the cationic form of Doxo electrostatically interacted with the native negative charges of GO-PEG-Fol (Table 1), allowing short-range π-π stacking.

The release profile of Doxo was studied using either PBS pH 7.4 or acetate buffer pH 5.5, which mimicked normal physiological medium and the tumour microenvironment, respectively. The study was carried out by equilibrium dialysis experiments, quantifying the amount of released doxorubicin in the external medium at scheduled time intervals and until 48 h (Figure 7). The drug release from GO-PEG-Fol/Doxo was compared to the diffusion profile of free Doxo, used as a control. Figure 7 shows that the diffusion of free drug at both pH values was not dependent on the medium and 100% of drug diffuses into the receiving compartment within 5 h.

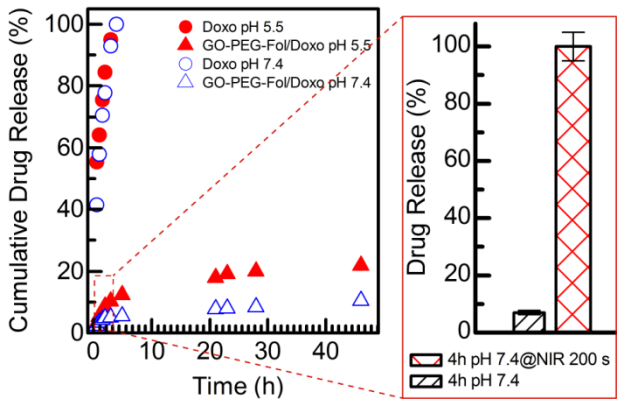

Figura 7. Drug release kinetics of GO-PEG-Fol/Doxo obtained at 37°C in PBS pH 7.4 and acetate buffer pH 5.5: the diffusion profile of free Doxo is reported as control experiments. The NIR-triggered drug release after 4h of incubation is reported on the right (power density = 7×10^{-2} W mm^{-3}).

GO-PEG-Fol/Doxo nanoflakes released their payload in a time-dependent fashion, without the burst effect observed for the free drug. Data also shows that only the 15 % of drug payload was released at pH 7.4 after 48 h of incubation, indicating good stability of the system upon administration, avoiding the premature drug release before reaching the target site. On the contrary, GO-PEG-Fol/Doxo released doxorubicin more quickly in acidic condition (~ 27 %), showing a remarkable pH-dependent release profile. One can speculate that, being GO-PEG-Fol highly carboxylated, the protonation of carboxylic

groups in acidic condition lead the partial dissociation of hydrogen bonding with Doxo molecules, which can freely diffuse throughout the tumour microenvironment.[47] Moreover, as the selective release of the drug payload can be in principle controlled photothermally by means of external NIR light stimuli, we also assessed the hyperthermia-triggered release after 4h of incubation (Figure 7, insert on the right).[10,48,49] This strategy is proposed to improve the selectivity of the treatment reducing toxic side effects. It can be noticed that just after 300 sec of laser treatment at low power density the nanosystem promptly released 100 % of its drug payload, indicating that the GO-PEG-Fol/Doxo can act as a technological platform capable of triggering simultaneously highly localized hyperthermia and on-demand drug release inside the tumour site. Hence, our nanosystem could be employed to gain synergistic and non-invasive photothermal effects to avoid drug resistance phenomena and efficiently eradicate solid tumours avoiding recidivisms.

3.3.3. Physicochemical stability of GO-PEG-Fol/Doxo in aqueous media.

The physicochemical stability of the GO-PEG-Fol/Doxo under physiological conditions was assessed both in PBS pH 7.4 and DMEM dispersion, at concentration of 0.1 mg mL^{-1}, by evaluating the size distribution over time (three days).

Table 2. Physiochemical stability of the GO-PEG-Fol/Doxo in aqueous dispersion at 37 °C

Medium	**[a]Size (nm)**			
	t = 0	t = 24h	t = 48h	t = 72h
PBS pH 7.4	48.0	48.2	51.4	64.2
DMEM	51.1	50.2	54.8	77.6

[a] Obtained by DLS analysis

Data reported in Table 2 showed that the size distribution of the Doxo-loaded nanosystem did not significantly change over time until three days of incubation at 37 °C. Indeed, the average diameter in PBS pH 7.4 passed

from 48 to 64.2 nm, indicating negligible aggregation of the GO nano-sheets. This trend was also observed in DMEM, where a slight aggregation was observed maybe due to the adsorption of proteins from the medium onto the GO-PEG-Fol surface. However, the original nanometric dimensions of the proposed nanosystem were preserved under physiological conditions, indicating a good stability.

3.4 Biological Characterization of the GO-PEG-Fol/Doxo nanoflakes.

3.4.1. In vitro cytotoxic effect on cancer and healthy cells.

The *in vitro* cytotoxicity of GO-PEG-Fol/Doxo was evaluated on breast cancer cells (MCF7 and MDA-MB-231) and healthy cells (HDFa), used as model of estrogen response, triple negative breast cancer cells and healthy cells, respectively, so as to evaluate the ability of the nanosystem to preferentially kill tumor cells instead of the healthy ones. In particular, to investigate the potential selectivity of GO-PEG-Fol/Doxo we used HDFa cell line, MCF-7 and MDA-MB-231 breast cancer cell lines as models that express variable levels of folic acid receptors (FR) on their cell surface. MDA-MB-231 is a highly FR positive human breast adenocarcinoma cell line that overexpresses FRs on their cell surfaces, whereas MCF-7 is a low FR expressing human breast adenocarcinoma cell line and HDFa is a normal cell line that does not express significant levels of FR on their cell surfaces.

In a first set of experiments GO-PEG-Fol was proven cytocompatible toward all cell lines considered both after 24 and 48 h of incubation (Figure 8a).

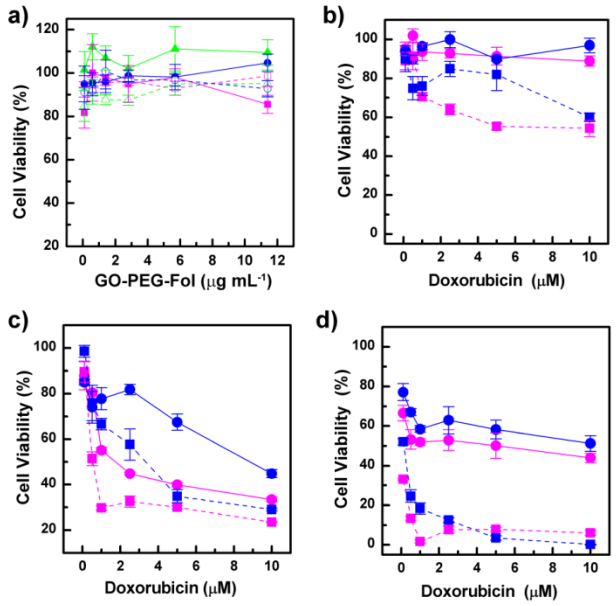

Figure 8. Cytocompatibility and *in vitro* anticancer effect. Cell viability of MCF7 (purple), MDA-MB-231 (green) and HDFa (blue) treated with GO-PEG-Fol for 24 (solid lines) and 48h (dashed lines) (a). Cell viability of HDFa (b), MCF7 (c) and MDA-MB-231 (d) treated with Doxorubicin (purple) and equivalent amount of GO-PEG-Fol/Doxo (blue) for 24 (solid lines) and 48 (dashed lines) hours.

The doxorubicin-loaded GO-PEG-Fol nano-flakes showed negligible cytotoxic effects on healthy HDFa, always lower if compared to that observed for equivalent amount of free Doxo (Table 2.: I_{max}^{48h} = 40±2.1 vs 45.7±4.2, respectively) (Figure 8b), whereas it displayed excellent antitumor activity against both breast cancer cells after 24 and 48 h of incubation (Figure 8c-d). However, GO-PEG-Fol/Doxo exhibited higher efficacy on MDA-MB-231 (FR+++), killing up to 99.8% of cells after 48 h of incubation at the higher concentration considered (10 μg mL^{-1}) (Figure 8d). As showed in Tab.2, GO-PEG-Fol/Doxo nanoflakes was forty times more efficacy on MDA-MB-231 cell lines, that overexpressed FR, compared to MCF7 cell lines (IC_{50}^{48h} ≈0,1vs 3.75μM, for MDA-MB-231 and MCF7, respectively). This finding hints at a crucial rule of folate-mediated endocytosis mechanisms which allows the selective cytotoxic effect observed for cancer cells that overexpress FR. The IC_{50} values reported in Table 2 for MCF7 are within the range reported for Doxo-loaded nanomedicines. To the best of our knowledge, prior works have reported IC_{50} from 3.4 to 18.25 μg mL^{-1}, confirming that

GO-PEG-Fol/Doxo nanoflakes have high pharmacological potency.[5,10,50] The same consideration can be made for MDA-MB-231 cells.[50–52] It is noteworthy that, comparable to the effect caused by free Doxo, GO-PEG-Fol/Doxo showed a selective cytotoxicity towards cancer cells, especially for MDA-MB-231. In fact, the selectivity index (SI) reported in Table 2, calculated as the ratio between the cytotoxic effect observed for cancer cells and HDFa at the maximum dose (I_{max}^{48h}), was significantly higher for the nanosystem if compared to that observed for free Doxo (2.5 vs 2.05). Despite this, a comparable SI was observed for free Doxo and GO-PEG-Fol/Doxo for MCF7 cells (1.78 vs 1.68). Some recent investigations have described doxorubicin-bound nanomaterials that lead to less effective *in vitro* cytotoxicity on HDFa (i.e., higher IC_{50}), but with lower selectivity index (SI<2.15).[10,11,53] This might be correlated to the higher folic acid (targeting agent) density displayed from the GO surface in GO-PEG-Fol/Doxo.

Table 2. Half maximal inhibitory concentration (IC_{50}) and maximum cell growth inhibition (I%) values calculated for free Doxo and GO-PEG-Fol/Doxo on HDFa, MCF7 and MDA-MB-231 cell lines.

Cell lines	Sample	$IC50^{24h}$ (μM)	I_{max}^{24h} (%)	$IC50^{48h}$ (μM)	I_{max}^{48h} (%)	SI
HDFa	Doxo	>10	17.1±2.5	>10	45.7±4.2	-
	GO-PEG-Fol/Doxo	>10	3.1±3.7	>10	40±2.1	-
MCF7	Doxo	1.72	66.5±0.9	0.57	76.6±0.3	1.68
	GO-PEG-Fol/Doxo	7.5	55.1±1.8	3.75	71±0.5	1.78
MDA-MB-231	Doxo	1.25	56.1±2.3	<0.1	94±1.3	2.05
	GO-PEG-Fol/Doxo	>10	48.8±3.9	≈0.1	99.8±0.2	2.50

3.4.2. In vitro cell uptake study on healthy fibroblasts and breast cancer cell lines.

With the aim of understanding if the nanosystem is able to enter cancer cells to act at intracellular level, we established cell uptake of GO-PEG-Fol/Doxo on HDFa, MCF7 and MDA-MB-231 by fluorescence microscopy up to 24 h of incubation. Free Doxo and GO-PEG-Fol/Doxo can be visualized upon cell internalization because of their inherent red fluorescence. Whilst bright red fluorescence was localized only inside nuclei up to 6 h from the incubation on HDFa, MCF7 and MDA-MB-231 displayed additional fluorescence inside cytosol and in the peri-nuclear region (Figure 9). A similar behavior was observed after 24 of incubation. On the whole, Figure 9 suggests that GO-PEG-Fol/Doxo enter HDFa and cancer cells exploiting different pathways, mainly influenced by the overexpression of FR, thus affecting the mode of action. In fact, MDA-MB-231 cells, which overexpress the higher level of FR on the cell membrane, are characterized by ubiquitously red fluorescence inside cells implying a different biodistribution of the nanosystem inside cells.

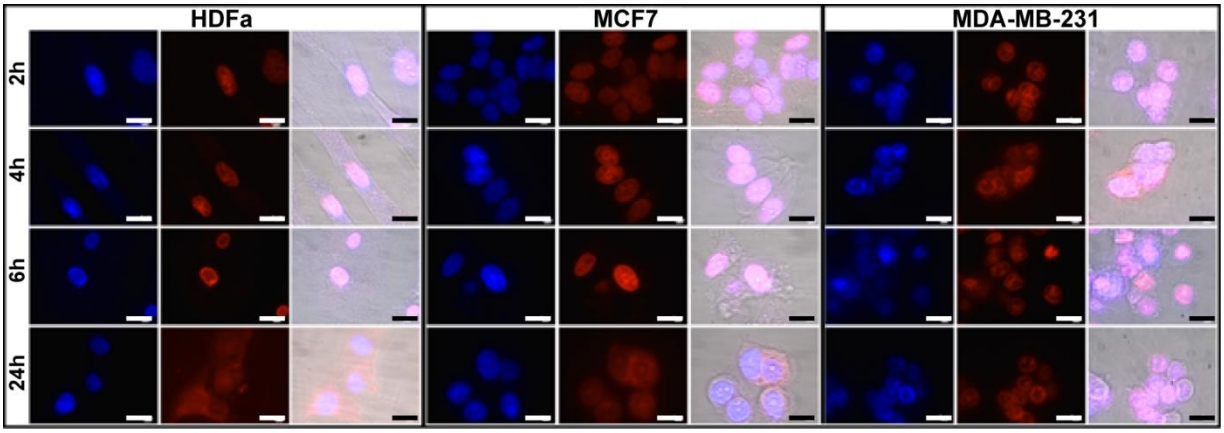

Figure 9. Uptake studies of GO-PEG-Fol/Doxo at Doxo concentration of 5μM on HDFa (FR-), MCF7 (FR++) and MDA-MB-231 (FR+++). Magnification 100x. Scale bar 50 μm

3.4.3. In vitro wound healing assay (cell migration test).

Migration is a critical characteristic of cancer cells for tumor burden and metastatic outbreak. An effective nanomedicine useful in precision cancer therapy should oppose metastasis by limiting cell

migration towards pre-metastatic niches, and wound healing assay could help us to study that potential inclination.[53,54] Cell migration was investigated on monolayered HDFa, MCF7 and MDA-MB-231 cell cultures incubated for 24 h with free Doxo at a drug concentration of 5μM or equivalent amount of GO-PEG-Fol/Doxo. Wound healing was quantified by taking into account the initial cell gap provoked by a scratch and the cell gap recovery in 24 h. GO-PEG-Fol/Doxo allowed the wound healing of HDFa culture after 24h, whereas free Doxo provided only 27 % healing after 48 h (Figure 10). This is in agreement to cell viability data (Figure 8b, Table 2), where a negligible dysfunction of the HDFa proliferation abilities was registered after the exposure with the nanosystem, whereas free Doxo provoked significant HDFa death. Interestingly, as migration processes were largely inhibited on both breast cancer cell lines treated with GO-PEG-Fol/Doxo or free Doxo a sharp decrease of wound healing was measured (from 0 to 37 % healing) (Figure 10). However, GO-PEG-Fol/Doxo exhibited higher inhibition activity on MDA-MB-231 (FR+++) cells after 48 h incubation (16 % healing), providing a good evidence that folic acid residues are key factors to promote Doxo anti-metastatic effects at intracellular level. Surprisingly, free Doxo did not elicit any effect on MDA-MB-231 cells.

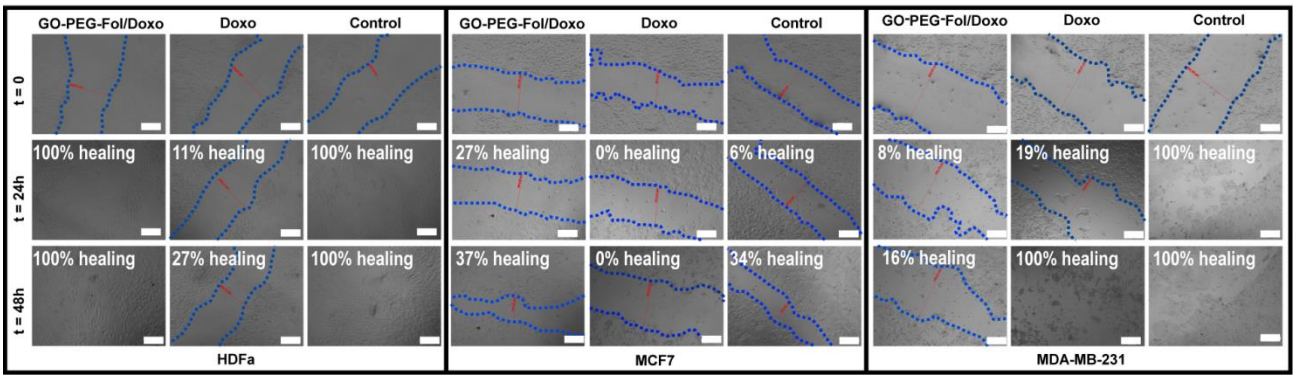

Figure 10. Wound healing assay at Doxo concentration of 5μM on HDFa, MCF7 and MDA-MB-231 cell lines by optical microscopy. Magnification 5x: scale bar 20 μm.

3.4.4. In vitro photothermal effect.

To demonstrate the applicability of the NIR photothermal ablation of cancer cells by means of GO-PEG-Fol/Doxo, we performed in *vitro* MTS assay on the healthy HDFa cell line and breast cancer cell

lines, which overexpress increasing amount of FR on the cell membrane (i.e. MCF7 and MDA-MB-231, respectively). The cell viability of the HDFa cells treated with either Doxo at a concentration range within 0.1 – 10 μM or equivalent amount of GO-PEG-Fol/Doxo did not significantly decrease after 24 h of incubation (Figure 11 a). The cell viability was found to slightly decrease to about 40% (50 and 38 % for the free Doxo and GO-PEG-Fol/Doxo, respectively) when the HDFa cells were also treated at the maximum Doxo dose with an 810 nm laser diode for 200 s at low power density (0.2 W cm^{-2}). This trend is clearly shown in the Live/Dead assay reported in Figure 11 a'-a''', where fibroblasts appear copious and healthy after the laser treatment both for free Doxo and the nanosystem. Things appear different if one looks the effect of the same treatment on both breast cancer cell lines (Figure 11 b-b''' and c-c'''). Cell viability sharply decreased with a dose-dependent trend after the NIR treatment both for Doxo and GO-PEG-Fol/Doxo on MCF7 and MDA-MB-231 (Figure 11 b and c). Although the NIR phototherapy improved free Doxo efficacy the IC_{50} values remained comparable, implying that the pharmacological potency of the free Doxo was not affected by the photothermal treatment. On the contrary, the potency of GO-PEG-Fol/Doxo remarkably increased after the NIR exposure (IC_{50} from 8.69 to 0.51 μM and from >10 to 1.88 μM for MCF7 and MDA-MB-231, respectively) (Figure 11 b,c). Besides, as shown in Figure 11 b-b''' and c-c''' the NIR photothermal efficacy of GO-PEG-Fol/Doxo was very higher than that of free Doxo, implying an excellent anticancer efficacy of this nanosystem compared to the free drug. In particular, for the GO-PEG-Fol/Doxo at the maximum dose cell viability reached 10 and 0.6% on MCF7 (Figure 11b) and MDA-MB-231 (Figure 11c), respectively, whereas the same dose of free Doxo led to cell viability values from 1.9 to 50 times higher. This is clearly shown in the Live/Dead experiments reported in Figure 11 b'-b''' and c'-c''', where live cell population appeared significantly lower after the NIR treatment on both cancer cell lines incubated with GO-PEG-Fol/Doxo (b''', c'''). It is noteworthy that the SI calculated for GO-PEG-Fol/Doxo considering photothermal effects (Figure 11 a-c) are about 12 and

2.3 times higher than that calculated for the free Doxo on MCF7 and MDA-MB-231, respectively. Corroborating the hypothesis that this nanosystem could enhance the efficacy of anticancer drugs by NIR-triggered localized hyperthermia, minimizing off-target toxic effects.

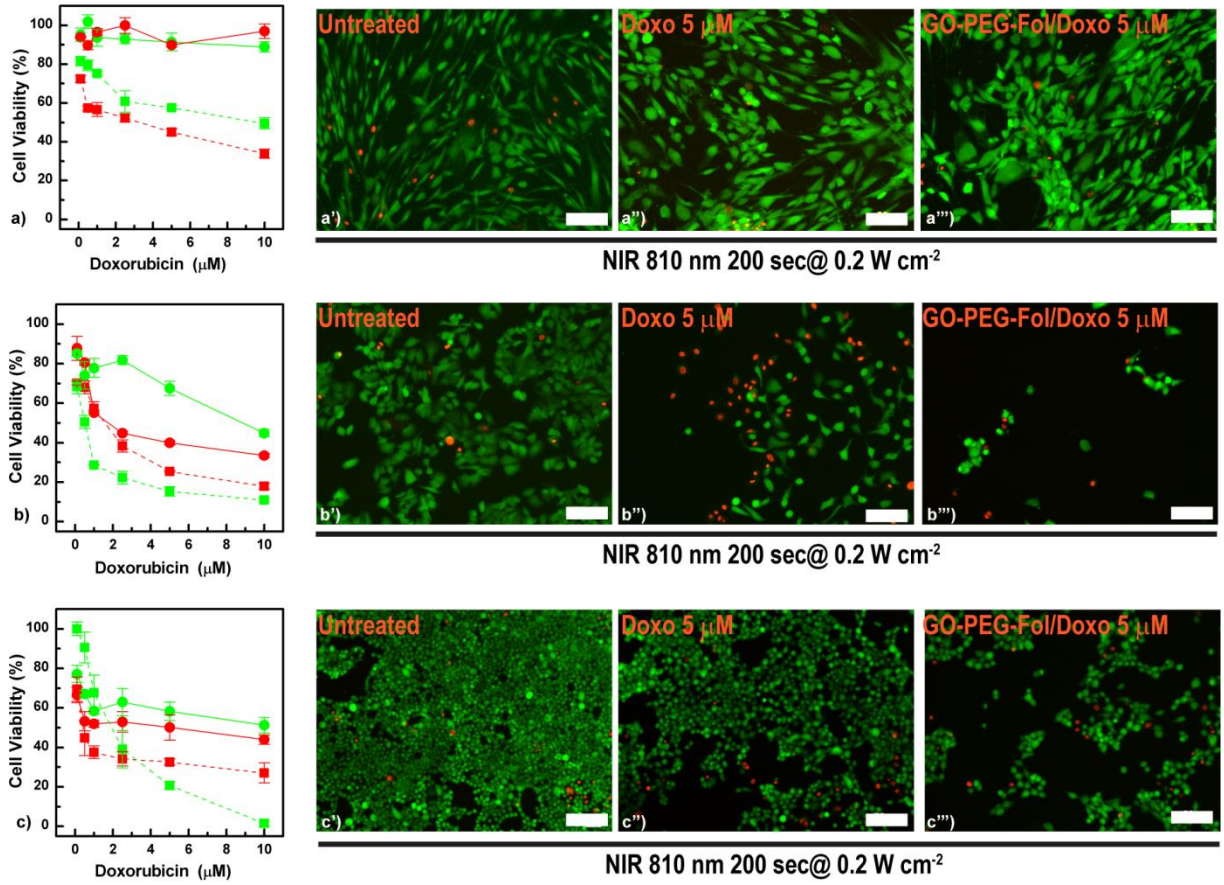

Figure 11. NIR photothermic effect on HDFa (a-a'''), MCF7 (b-b''') and MDA-MB-231 (c-c''') after the 810 nm laser exposure for 200 sec at low power density (0.2 W cm^{-2}). Cell viability (a, b, c) as function of Doxo concentration for free Doxo (red symbols) and GO-PEG-Fol/Doxo (green symbols) after 24 h of incubation (solid lines) followed by 810 nm laser treatment for 200 sec (dashed lines). Live/dead assay (a'-a'''; b'-b'''; c'-c'''): calcein-AM (green, live), ethidium homodimer-1 (red, dead). Magnification 5x: scale bar 100 μm.

4. Conclusions

GO represents a versatile 2-D carbon nanomaterial which may be promising in different biomedical applications due to their biocompatibility, adsorption and photothermal properties. Here, we developed

nano-sized folic acid-containing PEGylated GO, namely GO-PEG-Fol, as a therapeutic platform to combine stimuli-sensitive chemotherapy and photothermal therapy so as to improve breast cancer treatments, while reducing off-target side effects. We obtained azide-functionalized GO with small average size and narrow distribution, ~30 ±5 nm yielded via low-vacuum plasma etching. Highly folate functionalized GO nano-flakes were obtained by combining regioselective azide-alkyne click-chemistry and amide coupling between heterobifunctional Fol-PEG-alkyne or Fol-PEG-NH_2 chains with azide or carboxyl groups of GO-N_3, respectively. PEGylation of GO nano-flakes provoked 2-fold increase in the NIR absorbance and efficient photothermal conversion. Besides, the functionalization of GO with folic acid-containg PEG_{2000} chains provided cancer cell recognition capabilities and allowed loading high amounts of Doxo (>33% w/w), making it able to selectively enter and kill breast cancer cells overexpressing folic acid receptors. We assessed a selective *in vitro* photothermal cytotoxic effect on breast cancer cells (MCF7 and MDA-MB-231) from 3 to 12 times higher than that measured for healthy cells such as fibroblasts. Overall, we showed that GO-PEG-Fol could be exploited as a promising photothermal agent at low power density, owing to its targeting property, small size, suitable photothermal conversion, and selectivity towards breast cancer cells.

Acknowledgements

Part of this research was supported by the Fondazione Umberto Veronesi (FUV Fellowship 2018 and 2019). The authors declare no conflicts of interest associated to this manuscript. The Raman spectroscopy laboratory at ATeN Center, University of Palermo, is acknowledged for Raman equipment use.

References

[1] D. Wu, M. Si, H.-Y. Xue, H.-L. Wong, Nanomedicine applications in the treatment of breast cancer: Current state of the art, Int. J. Nanomedicine. (2017). doi:10.2147/IJN.S123437.

[2] H. Kennecke, R. Yerushalmi, R. Woods, M.C.U. Cheang, D. Voduc, C.H. Speers, T.O. Nielsen, K. Gelmon, Metastatic behavior of breast cancer subtypes, J. Clin. Oncol. (2010). doi:10.1200/JCO.2009.25.9820.

[3] O.A. Martin, R.L. Anderson, K. Narayan, M.P. MacManus, Does the mobilization of circulating tumour cells during cancer therapy cause metastasis?, Nat. Rev. Clin. Oncol. (2017). doi:10.1038/nrclinonc.2016.128.

[4] G. Giammona, G. Puglisi, B. Carlisi, R. Pignatello, A. Spadaro, A. Caruso, Polymeric prodrugs: α,β-poly(N-hydroxyethyl)-dl-aspartamide as a macromolecular carrier for some non-steroidal anti-inflammatory agents, Int. J. Pharm. (1989). doi:10.1016/0378-5173(89)90263-9.

[5] K. Vinothini, N.K. Rajendran, M.A. Munusamy, A.A. Alarfaj, M. Rajan, Development of biotin molecule targeted cancer cell drug delivery of doxorubicin loaded κ-carrageenan grafted graphene oxide nanocarrier, Mater. Sci. Eng. C. (2019). doi:10.1016/j.msec.2019.03.011.

[6] M.W. Tibbitt, J.E. Dahlman, R. Langer, Emerging Frontiers in Drug Delivery, J. Am. Chem. Soc. (2016). doi:10.1021/jacs.5b09974.

[7] R.X. Zhang, H.L. Wong, H.Y. Xue, J.Y. Eoh, X.Y. Wu, Nanomedicine of synergistic drug combinations for cancer therapy – Strategies and perspectives, J. Control. Release. (2016). doi:10.1016/j.jconrel.2016.06.012.

[8] P.M. Enriquez-Navas, J.W. Wojtkowiak, R.A. Gatenby, Application of evolutionary principles to cancer therapy, Cancer Res. (2015). doi:10.1158/0008-5472.CAN-15-1337.

[9] C. Huang, J. Wu, W. Jiang, R. Liu, Z. Li, Y. Luan, Amphiphilic prodrug-decorated graphene oxide as a multi-functional drug delivery system for efficient cancer therapy, Mater. Sci. Eng. C. (2018). doi:10.1016/j.msec.2018.03.017.

[10] N. Mauro, C. Scialabba, G. Cavallaro, M. Licciardi, G. Giammona, Biotin-containing reduced graphene oxide-based nanosystem as a multieffect anticancer agent: Combining hyperthermia with targeted chemotherapy, Biomacromolecules. 16 (2015) 2766–2775. doi:10.1021/acs.biomac.5b00705.

[11] N. Mauro, A.L. Volsi, C. Scialabba, M. Licciardi, G. Cavallaro, G. Giammona, Photothermal ablation of cancer cells using folate-coated gold/graphene oxide composite, Curr. Drug Deliv. 14 (2017). doi:10.2174/1567201813666160520113804.

[12] J.T. Robinson, S.M. Tabakman, Y. Liang, H. Wang, H. Sanchez Casalongue, D. Vinh, H. Dai, Ultrasmall reduced graphene oxide with high near-infrared absorbance for photothermal therapy, J. Am. Chem. Soc. (2011). doi:10.1021/ja2010175.

[13] C.C. Liu, J.J. Zhao, R. Zhang, H. Li, B. Chen, L.L. Zhang, H. Yang, Multifunctionalization of graphene and graphene oxide for controlled release and targeted delivery of anticancer drugs, Am. J. Transl. Res. (2017).

[14] X. Zhao, Z. Wei, Z. Zhao, Y. Miao, Y. Qiu, W. Yang, X. Jia, Z. Liu, H. Hou, Design and Development of Graphene Oxide Nanoparticle/Chitosan Hybrids Showing pH-Sensitive Surface Charge-Reversible Ability for Efficient Intracellular Doxorubicin Delivery, ACS Appl. Mater. & Interfaces. 10 (2018) 6608–6617. doi:10.1021/acsami.7b16910.

[15] H. Tiwari, N. Karki, M. Pal, S. Basak, R.K. Verma, R. Bal, N.D. Kandpal, G. Bisht, N.G. Sahoo, Functionalized graphene oxide as a nanocarrier for dual drug delivery applications: The synergistic effect of quercetin and gefitinib against ovarian cancer cells, Colloids Surfaces B Biointerfaces. (2019). doi:10.1016/j.colsurfb.2019.03.037.

[16] N. Mauro, A. Li Volsi, C. Scialabba, M. Licciardi, G. Cavallaro, G. Giammona, Photothermal

ablation of cancer cells using folate-coated gold/grapheme oxide composite, Curr. Drug Deliv. 13 (2016) 1–1. doi:10.2174/1567201813666160520113804.

[17] C. Fiorica, N. Mauro, G. Pitarresi, C. Scialabba, F.S. Palumbo, G. Giammona, Double-Network-Structured Graphene Oxide-Containing Nanogels as Photothermal Agents for the Treatment of Colorectal Cancer, Biomacromolecules. 18 (2017) 1010–1018. doi:10.1021/acs.biomac.6b01897.

[18] N. Mauro, C. Scialabba, G. Pitarresi, G. Giammona, Enhanced adhesion and in situ photothermal ablation of cancer cells in surface-functionalized electrospun microfiber scaffold with graphene oxide, Int. J. Pharm. 526 (2017). doi:10.1016/j.ijpharm.2017.04.045.

[19] D. Dorniani, B. Saifullah, F. Barahuie, P. Arulselvan, M.Z. Bin Hussein, S. Fakurazi, L.J. Twyman, Graphene Oxide-Gallic Acid Nanodelivery System for Cancer Therapy, Nanoscale Res. Lett. (2016). doi:10.1186/s11671-016-1712-2.

[20] X. Xu, J. Wang, Y. Wang, L. Zhao, Y. Li, C. Liu, Formation of graphene oxide-hybridized nanogels for combinative anticancer therapy, Nanomedicine Nanotechnology, Biol. Med. (2016). doi:10.1016/j.nano.2017.05.007.

[21] Z. Liu, J.T. Robinson, X. Sun, H. Dai, PEGylated nanographene oxide for delivery of water-insoluble cancer drugs, J. Am. Chem. Soc. (2008). doi:10.1021/ja803688x.

[22] N.H. Park, W. Cheng, F. Lai, C. Yang, P. Florez De Sessions, B. Periaswamy, C. Wenhan Chu, S. Bianco, S. Liu, S. Venkataraman, Q. Chen, Y.Y. Yang, J.L. Hedrick, Addressing Drug Resistance in Cancer with Macromolecular Chemotherapeutic Agents, J. Am. Chem. Soc. (2018). doi:10.1021/jacs.7b11468.

[23] S.N. Bhatia, G. von Maltzahn, J.H. Park, A. Agrawal, N.K. Bandaru, S.K. Das, M.J. Sailor,

Computationally Guided Photothermal Tumor Therapy Using Long-Circulating Gold Nanorod Antennas, Cancer Res. (2009).

[24] L. Tong, Q. Wei, A. Wei, J.X. Cheng, Gold nanorods as contrast agents for biological imaging: Optical properties, surface conjugation and photothermal effects, Photochem. Photobiol. (2009). doi:10.1111/j.1751-1097.2008.00507.x.

[25] F. Zhou, D. Xing, Z. Ou, B. Wu, D.E. Resasco, W.R. Chen, Cancer photothermal therapy in the near-infrared region by using single-walled carbon nanotubes, J. Biomed. Opt. (2009). doi:10.1117/1.3078803.

[26] S. Ghosh, S. Dutta, E. Gomes, D. Carroll, R. D'Agostino, J. Olson, M. Guthold, W.H. Gmeiner, Increased heating efficiency and selective thermal ablation of malignant tissue with DNA-encased multiwalled carbon nanotubes, ACS Nano. (2009). doi:10.1021/nn900368b.

[27] K. Ghosal, A. Ghosh, Carbon dots: The next generation platform for biomedical applications, Mater. Sci. Eng. C. (2019). doi:10.1016/j.msec.2018.11.060.

[28] S. Gurunathan, J.W. Han, E.S. Kim, J.H. Park, J.H. Kim, Reduction of graphene oxide by resveratrol: A novel and simple biological method for the synthesis of an effective anticancer nanotherapeutic molecule, Int. J. Nanomedicine. (2015). doi:10.2147/IJN.S79879.

[29] M.H. Lim, I.C. Jeung, J. Jeong, S.J. Yoon, S.H. Lee, J. Park, Y.S. Kang, H. Lee, Y.J. Park, H.G. Lee, S.J. Lee, B.S. Han, N.W. Song, S.C. Lee, J.S. Kim, K.H. Bae, J.K. Min, Graphene oxide induces apoptotic cell death in endothelial cells by activating autophagy via calcium-dependent phosphorylation of c-Jun N-terminal kinases, Acta Biomater. (2016). doi:10.1016/j.actbio.2016.09.018.

[30] G.Y. Chen, C.L. Chen, H.Y. Tuan, P.X. Yuan, K.C. Li, H.J. Yang, Y.C. Hu, Graphene oxide

triggers toll-like receptors/autophagy responses in vitro and inhibits tumor growth in vivo, Adv. Healthc. Mater. (2014). doi:10.1002/adhm.201300591.

[31] T. Zhou, B. Zhang, P. Wei, Y. Du, H. Zhou, M. Yu, L. Yan, W. Zhang, G. Nie, C. Chen, Y. Tu, T. Wei, Energy metabolism analysis reveals the mechanism of inhibition of breast cancer cell metastasis by PEG-modified graphene oxide nanosheets, Biomaterials. (2014). doi:10.1016/j.biomaterials.2014.08.033.

[32] S. Eigler, Y. Hu, Y. Ishii, A. Hirsch, Controlled functionalization of graphene oxide with sodium azide, Nanoscale. (2013). doi:10.1039/c3nr04332k.

[33] P.C. Griffiths, N. Mauro, D.M. Murphy, E. Carter, S.C.W. Richardson, P. Dyer, P. Ferruti, Self-assembled PAA-based nanoparticles as potential gene and protein delivery systems, Macromol. Biosci. 13 (2013) 641–649. doi:10.1002/mabi.201200462.

[34] M. Licciardi, A. Li Volsi, N. Mauro, C. Scialabba, G. Cavallaro, G. Giammona, M. Licciardi, A. Li Volsi, N. Mauro, C. Scialabba, G. Cavallaro, G. Giammona, Preparation and Characterization of Inulin Coated Gold Nanoparticles for Selective Delivery of Doxorubicin to Breast Cancer Cells, J. Nanomater. 2016 (2016) 1–12. doi:10.1155/2016/2078315.

[35] T. Ishii, M. Yamada, T. Hirase, Y. Nagasaki, New Synthesis of Heterobifunctional Poly(ethylene glycol) Possessing a Pyridyl Disulfide at One End and a Carboxylic Acid at the Other End, Polym. J. 37 (2005) 221–228. doi:10.1295/polymj.37.221.

[36] C. Scialabba, R. Puleio, D. Peddis, G. Varvaro, P. Calandra, G. Cassata, L. Cicero, M. Licciardi, G. Giammona, Folate targeted coated SPIONs as efficient tool for MRI, Nano Res. 10 (2017) 3212–3227. doi:10.1007/s12274-017-1540-4.

[37] V. Du Nguyen, H.-K. Min, C.-S. Kim, J. Han, J.-O. Park, E. Choi, Folate receptor-targeted

liposomal nanocomplex for effective synergistic photothermal-chemotherapy of breast cancer in vivo, Colloids Surfaces B Biointerfaces. 173 (2019) 539–548. doi:10.1016/j.colsurfb.2018.10.013.

[38] P.E. Saw, J. Park, E. Lee, S. Ahn, J. Lee, H. Kim, J. Kim, M. Choi, O.C. Farokhzad, S. Jon, Effect of PEG pairing on the efficiency of cancer-targeting liposomes, Theranostics. (2015). doi:10.7150/thno.10732.

[39] P. Ferruti, N. Mauro, A. Manfredi, E. Ranucci, Hetero-difunctional dimers as building blocks for the synthesis of poly(amidoamine)s with hetero-difunctional chain terminals and their derivatives, J. Polym. Sci. Part A Polym. Chem. 50 (2012). doi:10.1002/pola.26325.

[40] S. Eigler, Y. Hu, Y. Ishii, A. Hirsch, Controlled functionalization of graphene oxide with sodium azide, Nanoscale. (2013). doi:10.1039/c3nr04332k.

[41] A. Kaniyoor, S. Ramaprabhu, A Raman spectroscopic investigation of graphite oxide derived graphene, AIP Adv. (2012). doi:10.1063/1.4756995.

[42] M.K. Kumawat, M. Thakur, R. Bahadur, T. Kaku, R.S. Prabhuraj, A. Ninawe, R. Srivastava, Preparation of graphene oxide-graphene quantum dots hybrid and its application in cancer theranostics, Mater. Sci. Eng. C. (2019). doi:10.1016/j.msec.2019.109774.

[43] L. Wang, D. Yu, R. Dai, D. Fu, W. Li, Z. Guo, C. Cui, J. Xu, S. Shen, K. Ma, PEGylated doxorubicin cloaked nano-graphene oxide for dual-responsive photochemical therapy, Int. J. Pharm. (2019). doi:10.1016/j.ijpharm.2018.12.037.

[44] A. Bahreyni, R. Yazdian-Robati, S. Hashemitabar, M. Ramezani, P. Ramezani, K. Abnous, S.M. Taghdisi, A new chemotherapy agent-free theranostic system composed of graphene oxide nano-complex and aptamers for treatment of cancer cells, Int. J. Pharm. (2017).

doi:10.1016/j.ijpharm.2017.05.014.

[45] M. Zhang, R.R. Naik, L. Dai, eds., Carbon Nanomaterials for Biomedical Applications, Springer International Publishing, Cham, 2016. doi:10.1007/978-3-319-22861-7.

[46] S. Wu, X. Zhao, Y. Li, Q. Du, J. Sun, Y. Wang, X. Wang, Y. Xia, Z. Wang, L. Xia, Adsorption properties of doxorubicin hydrochloride onto graphene oxide: Equilibrium, kinetic and thermodynamic studies, Materials (Basel). (2013). doi:10.3390/ma6052026.

[47] M. Rezaian, R. Maleki, M. Dahri Dahroud, A. Alamdari, M. Alimohammadi, pH-Sensitive Co-Adsorption/Release of Doxorubicin and Paclitaxel by Carbon Nanotube, Fullerene, and Graphene Oxide in Combination with N-isopropylacrylamide: A Molecular Dynamics Study, Biomolecules. 8 (2018) 127. doi:10.3390/biom8040127.

[48] C. Scialabba, A. Sciortino, F. Messina, G. Buscarino, M. Cannas, G. Roscigno, G. Condorelli, G. Cavallaro, G. Giammona, N. Mauro, Highly Homogeneous Biotinylated Carbon Nanodots: Red-emitting Nano-heaters as Theranostic Agents Towards Precision Cancer Medicine, ACS Appl. Mater. Interfaces. (2019). doi:10.1021/acsami.9b04925.

[49] X. Bao, Y. Yuan, J. Chen, B. Zhang, D. Li, D. Zhou, P. Jing, G. Xu, Y. Wang, K. Holá, D. Shen, C. Wu, L. Song, C. Liu, R. Zbořil, S. Qu, In vivo theranostics with near-infrared-emitting carbon dots—highly efficient photothermal therapy based on passive targeting after intravenous administration, Light Sci. Appl. (2018). doi:10.1038/s41377-018-0090-1.

[50] J. Chen, M. Shi, P. Liu, A. Ko, W. Zhong, W.J. Liao, M.M.Q. Xing, Reducible polyamidoamine-magnetic iron oxide self-assembled nanoparticles for doxorubicin delivery, Biomaterials. (2014). doi:10.1016/j.biomaterials.2013.10.057.

[51] H. Song, J. Zhang, W. Wang, P. Huang, Y. Zhang, J. Liu, C. Li, D. Kong, Acid-responsive

PEGylated doxorubicin prodrug nanoparticles for neuropilin-1 receptor-mediated targeted drug delivery, Colloids Surfaces B Biointerfaces. (2015). doi:10.1016/j.colsurfb.2015.09.030.

[52] D. Ren, F. Kratz, S.W. Wang, Protein nanocapsules containing doxorubicin as a pH-responsive delivery system, Small. (2011). doi:10.1002/smll.201002242.

[53] N. Mauro, C. Scialabba, R. Puleio, P. Varvarà, M. Licciardi, G. Cavallaro, G. Giammona, SPIONs embedded in polyamino acid nanogels to synergistically treat tumor microenvironment and breast cancer cells, Int. J. Pharm. 555 (2019) 207–219. doi:10.1016/j.ijpharm.2018.11.046.

[54] Y. Kam, C. Guess, L. Estrada, B. Weidow, V. Quaranta, A novel circular invasion assay mimics in vivo invasive behavior of cancer cell lines and distinguishes single-cell motility in vitro, BMC Cancer. (2008). doi:10.1186/1471-2407-8-198.

TOC